Gas-Phase Ion-Mobility Characterization of SAM-Functionalized Au Nanoparticles

D-H. Tsai,[†,‡] R. A. Zangmeister,[‡] L. F. Pease III,[‡] M. J. Tarlov,[‡] and M. R. Zachariah*[,†,‡]

Department of Chemistry and Biochemistry, and Department of Mechanical Engineering, University of Maryland, College Park, Maryland, and National Institute of Standards and Technology, Gaithersburg, Maryland

We present results of a systematic examination of functionalized gold nanoparticles (Au-NPs) by electrospray-differential mobility analysis (ES-DMA). Commercially available, citrate-stabilized Au colloid solutions (10–60 nm) were sized using ES-DMA, from which changes in particle size of less than 0.3 nm were readily discerned. It was found that the formation of salt particles and the coating of Au-NPs by salt during the electrospray process can interfere with the mobility analysis, which required the development of sample preparation and data correction protocols to extract correct values for the Au-NP size. Formation of self-assembled monolayers (SAMs) of alkanethiol molecules on the Au-NP surface was detected from a change in particle mobility, which could be modeled to extract the surface packing density of SAMs. A gas-phase temperature-programmed desorption (TPD) kinetic study of SAMs on Au-NPs found the data to be consistent with a second-order Arrhenius-based rate law, yielding an Arrhenius factor of 1.0×10^{11} s^{-1} and an activation energy $\sim$105 kJ/mol. For the size range of SAM-modified Au-NP we considered, the effect of surface curvature on the energetics of binding of carboxylic acid terminated SAMs is evidently negligible, with binding energies determined by TPD agreeing with those reported for the same SAMs on planar surfaces. This study suggests that the ES-DMA can be added to the tool set of characterization methods used to study the structure and properties of coated nanoparticles.

1. Introduction

Gold nanoparticles (Au-NPs) are being widely considered for many applications in biosensing and health diagnostics due in large part to their unique optical properties.[1,2] Au-NPs can also be readily modified with alkanethiol self-assembled monolayers (SAMs) for precise control of their surface chemical and physical properties.[3–5] The wide range of available terminal functional groups of SAMs enables facile attachment of biological molecules such as proteins, nucleic acids,[6] and carbohydrates. One exemplary application of surface-modified Au-NPs is for the diagnosis and treatment of cancers.[2,7] For such applications, desirable properties of the functional Au-NPs include (1) high purity, (2) monodisperse size, and (3) well-controlled adsorption/release of materials from the surface or interior of nanoparticles.

A significant challenge in using Au-NPs, or any engineered nanoparticles, for clinical diagnostics or as therapeutics in humans will be their characterization. An important aspect of regulatory approval for use in humans will include rigorous physical and chemical characterization of the nanoparticle measuring properties such as the physical size of the particle, the size distribution, particle structure, and the composition of chemical or biological coatings. It is unlikely that one analytical technology will be able to answer all these questions; instead, characterization will likely entail the application of complementary, orthogonal methods to give a clear picture of the physical and chemical profile of engineered nanoparticles.

In this paper we describe the use of electrospray-differential mobility analysis (ES-DMA) for characterizing engineered nanoparticles. We focus on the determination of the surface packing density and strength of binding of alkanethiol SAMs on Au-NPs. The approach taken is to apply electrospray (ES) followed by ion-mobility characterization (gas-phase electrophoresis). A gas-phase approach is used for many of the same reasons that ES-mass spectrometry (ES-MS) approaches are used so extensively in the proteomics research community. It is a clean, continuous process that readily charges the nanoparticles which can in turn be easily size-classified on the basis of their mobility.[8,9] We present here an approach to electrospray alkanethiol-functionalized gold nanoparticles and characterize the size and coating stability of these conjugated Au nanoparticles by differential mobility analysis (DMA). We demonstrate the utility of the method by measuring the coating thickness of the SAM and use a programmed thermal environment in the gas phase to determine the binding energy of the thiol monolayers as a function of particle size.

* To whom correspondence should be addressed. E-mail: mrz@umd.edu.

† University of Maryland.

‡ National Institute of Standards and Technology.

(1) Talley, C. E.; Jackson, J. B.; Oubre, C.; Grady, N. K.; Hollars, C. W.; Lane, S. M.; Huser, T. R.; Nordlander, P.; Halas, N. J. *Nano Lett.* **2005**, *5*(8), 1569–1574, Surface-enhanced Raman scattering from individual Au nanoparticles and nanoparticle dimer substrates.

(2) West, J. L.; Halas, N. J. *Ann. Rev. Biomed. Eng.* **2003**, *5*, 285–292, Engineered nanomaterials for biophotonics applications: Improving sensing, imaging, and therapeutics.

(3) Sandhyarani, N.; Pradeep, T. *Int. Rev. Phys. Chem.* **2003**, *22*(2), 221–262, Current understanding of the structure, phase transitions and dynamics of self-assembled monolayers on two- and three-dimensional surfaces.

(4) Weisbecker, C. S.; Merritt, M. V.; Whitesides, G. M. *Langmuir* **1996**, *12*(16), 3763–3772, Molecular self-assembly of aliphatic thiols on gold colloids.

(5) Henz, B.; T. H.; Zachariah, M. R. *Langmuir* **2007**, Mechano-Chemical Stability of Gold Nanoparticles Coated with Alkanethiolate SAM's.

(6) Pease, L.; Zangmeister, R.; Zachariah, M. R.; Tarlov, M. J. *J. Phys. Chem. C* **2007**, Quantifying the Surface Coverage of Conjugate Molecules on Functionalized Nanoparticles.

(7) Paciotti, G. F.; Myer, L.; Weinreich, D.; Goia, D.; Pavel, N.; McLaughlin, R. E.; Tamarkin, L. *Drug Delivery* **2004**, *11*(3), 169–183, Colloidal gold: A novel nanoparticle vector for tumor directed drug delivery.

(8) Tsai, D. H.; Hawa, T.; Kan, H. C.; Phaneuf, R. J.; Zachariah, M. R. *Nanotechnology* **2007**, *18*(36), -Spatial and size-resolved electrostatic-directed deposition of nanoparticles on a field-generating substrate: theoretical and experimental analysis.

(9) Grobelny, J.; Tsai, D. H.; Kim, D. I.; Pradeep, N.; Cook, R. F.; Zachariah, M. R. *Nanotechnology* **2006**, *17*(21), 5519–5524, Mechanism of nanoparticle manipulation by scanning tunnelling microscopy.

2. Experimental Section

Electrospray (ES) of Au-NPs from solution is a promising method for generating individual aerosol nanoparticles for DMA. Although the ES of unconjugated[10,11] and conjugated[12–15] Au-NPs has very recently been demonstrated, the studies reported here are, to our knowledge, the first demonstration of ES-DMA to characterize conjugated NPs. ES of clean Au nanoparticles remains challenging because the presence of salts or surfactants, typically added to stabilize the colloid, can result in the formation of salt particles during ES that interfere with the DMA measurement. Furthermore, for stable cone-jet operation, the solution conductivity must be precisely controlled.

2.1. Materials. In preparing the functionalized Au-NPs for measurement by ES-DMA, we first needed to understand how the presence of additives that serve to stabilize the colloids could potentially bias ES-DMA results and then to develop sample preparation protocols to minimize the deleterious effect of these additives. Commercially available, monodisperse Au colloids (10, 20, 30, and 60 nm, citrate-stabilized, Ted Pella Inc.) were used in this work. Alkanethiols of 11-mercaptoundecanoic acid (99+%, MUA, Asemblon, Inc.) and (1-mercapto-11-undecyl)tri(ethyleneglycol) (99+%, TEG, Asemblon, Inc.) were chosen as models of charged and neutral, respectively, self-assembled monolayers (SAMs) on Au nanoparticles. Conjugated Au colloids were prepared using 5 times excess the amount of thiol needed to form a full monolayer on the Au colloids as approximated using a surface density of 5×10^{14} molecules/cm^2 [16] and total gold colloid surface area based on vendor provided information. The alkanethiols were added to 1 mL aliquots of the as-received Au colloids at a concentration of 10 μmol/L and allowed to react for 20 h. The Au colloid solution was then centrifuged to separate the colloids from the supernatant containing excess stabilizer and thiols. The supernatant was removed and replaced with an equivalent volume of aqueous ammonium acetate (99.9%) solution ($\sim$2.5 mmol/L, 0.03 S/m). The Au colloids then were easily dispersed by mixing. Additional characterization of the SAM/Au colloid conjugates was performed using Fourier transform infrared spectroscopy (FTIR) and X-ray photoelectron spectroscopy (XPS).

2.2. FTIR, XPS, and TEM Analysis. Conjugated Au colloids were concentrated by centrifugation and then dried on commercially available Teflon cards for FTIR and indium foil for XPS. XPS was performed with an AXIS Ultra[DLD] (Kratos Analytical, Manchester, UK) and FTIR with a FTS 7000 series spectrometer (Bio-Rad Laboratories, Digilab Division, Cambridge, MA). Transmission FTIR absorption spectra were measured using a cryogenic mercury cadmium telluride detector. Presented FTIR spectra are the result of averaging 128 scans at 4 cm^{-1} resolution. XPS measurements were made with monochromatic Al Kα radiation at an X-ray power of 150 W. High-resolution scans were acquired for Au 4f, S 2p, and C1s regions in the fixed analyzer transmission mode with pass energy of 40 eV. All FTIR and XPS measurements were performed on freshly prepared samples. FTIR and XPS spectral analysis are described in the Supporting Information.

Figure 1. Schematic of experimental system, including differential mobility analyzer (DMA) and condensation particle counter (CPC).

Additionally, Au-NPs generated from the ES process were directly deposited on transmission electron microscopy (TEM) grids with an electrostatic precipitator[9,17] to enable TEM characterization. Conjugated Au-NPs were collected directly from the dried Au colloids onto TEM grids.

2.3. Electrospray Particle Generation and Differential Mobility Analysis. Figure 1 represents a schematic diagram of our experimental system, consisting of an electrospray aerosol generator (Model 3480, TSI Inc.), a differential mobility analyzer column (Model 3080n, TSI Inc.), and a condensation particle counter (CPC, Model 3025, TSI Inc.). Flow handling to the DMA column and the interface of the instruments employed a home-built design. Conductive solutions of Au colloids were placed in the pressure chamber and then delivered to the nozzle through a capillary (0.025 mm in diameter, 24 cm in length. TSI Inc.).[18] The liquid flow rate, Q_1, was $\sim$66 nL/min, and the flow rate of carrier gas was 1.2 L/min. To achieve better electrical stability in the ES, the filtered air was mixed with CO$_2$ (83% air and 17% CO$_2$).[19] Operating with an applied voltage ranging between +2 and 3 kV, the Au colloids were sprayed in a cone-jet mode as highly positively charged aerosolized droplets in the gas phase. By passing the aerosol stream through a housing containing an α-radioactive Po-210 source, these highly charged droplets collided with bipolarly charged ions, thereby reducing their charges to a Boltzmann distribution. Consequently, most droplets dried into particles with a single net charge and were directly passed to the differential mobility analyzer (DMA) for particle size measurement and counted with the CPC. The diameter of Au-NP, d_p, was characterized by electrical mobility, which is inversely proportional to the projected area of the particle. In order to have sufficient resolution and stability in the DMA measurements,[20] the sheath flow of the DMA was set to 30 Lpm for the 10–30 nm sized particles, and 10 Lpm for the 60 nm particles. On the basis of the operating conditions of the DMA, the theoretical full width at half-maximum (FWHM) in the size distribution[21] gives us 10 $\pm$ 0.2 nm for 10 nm particles, 20 $\pm$ 0.3 nm for 20 nm particles, 30 $\pm$ 0.5 nm for 30 nm particles, and 60 $\pm$ 3 nm for 60 nm particles. To obtain a precise size distribution, the scanning step size was 0.2 nm. Because

(10) Bottger, P. H. M.; Bi, Z.; Adolph, D.; Dick, K. A.; Karlsson, L. S.; Karlsson, M. N. A.; Wacaser, B. A.; Deppert, K. *Nanotechnology* **2007**, *18*(10), -Electrospraying of colloidal nanoparticles for seeding of nanostructure growth.

(11) Lenggoro, I. W.; Widiyandari, H.; Hogan, C. J.; Biswas, P.; Okuyama, K. *Anal. Chim. Acta* **2007**, *585*(2), 193–201, Colloidal nanoparticle analysis by nanoelectrospray size spectrometry with a heated flow.

(12) Tracy, J. B.; Kalyuzhny, G.; Crowe, M. C.; Balasubramanian, R.; Choi, J. P.; Murray, R. W. *J. Am. Chem. Soc.* **2007**, *129*(21), 6706−+Poly(ethylene glycol) ligands for high-resolution nanoparticle mass spectrometry.

(13) Schaaff, T. G.; Whetten, R. L. *J. Phys. Chem. B* **2000**, *104*(12), 2630–2641, Giant gold-glutathione cluster compounds: Intense optical activity in metal-based transitions.

(14) Schaaff, T. G. *Anal. Chem.* **2004**, *76*(21), 6187–6196, Laser desorption and matrix-assisted laser desorption/ionization mass spectrometry of 29-kDa Au:SR cluster compounds.

(15) Gies, A. P.; Hercules, D. M.; Gerdon, A. E.; Cliffel, D. E. *J. Am. Chem. Soc.* **2007**, *129*(5), 1095–1104, Electrospray mass spectrometry study of tiopronin monolayer-protected gold nanoclusters.

(16) Love, J. C.; Estroff, L. A.; Kriebel, J. K.; Nuzzo, R. G.; Whitesides, G. M. *Chem. Rev.* **2005**, *105*(4), 1103–1169, Self-assembled monolayers of thiolates on metals as a form of nanotechnology.
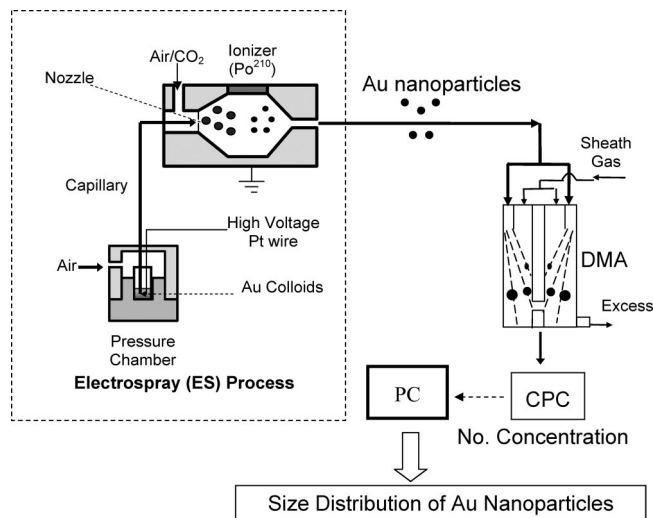
(17) *TSI Model 3089 Electrostatic Aerosol Sampler Menu* TSI inc.

(18) *TSI Model 3480 Electrospray Aerosol Generator Menu* TSI inc.

(19) Lenggoro, I. W.; Xia, B.; Okuyama, K.; de la Mora, J. F. *Langmuir* **2002**, *18*(12), 4584–4591, Sizing of colloidal nanoparticles by electrospray and differential mobility analyzer methods.

(20) Kim, J. H.; Mulholland, G. W.; Kukuck, S. R.; Pui, D. Y. H. *J. Res. Natl. Inst. Stand. Technol.* **2005**, *110*(1), 31–54, Slip correction measurements of certified PSL nanoparticles using a nanometer differential mobility analyzer (nano-DMA) for Knudsen number from 0.5 to 83.

(21) Chen, D. R.; Pui, D. Y. H.; Hummes, D.; Fissan, H.; Quant, F. R.; Sem, G. J. *J. Aerosol Sci.* **1998**, *29*(5–6), 497–509, Design and evaluation of a nanometer aerosol differential mobility analyzer (Nano-DMA).

of the stability of DMA measurements, we were able to resolve a change in diameter as small as 0.2 nm.[22,23]

Because we do not directly evaluate the droplet size generated from the ES source, we employ a scaling law for estimation purposes. The initial ES droplet size can be evaluated by

$$D_d = D_{d,0} \times \left(\frac{Q_1 K_0}{Q_0 K_1} \right)^{\frac{1}{3}} \tag{1}$$

where Q_0 is the flow rate, K_0 is the conductivity of the colloidal solution and $D_{d,0}$ is the estimated droplet size ($\sim$160 nm).[24] In our work the conductivity of Au colloids, K_1, was 0.03 S/m. Hence, the calculated droplet size using this scaling rule is $\sim$300 nm.

3. Result and Discussion

Our objective is to develop a systematic approach for characterizing SAM-conjugated Au-NPs based on gas-phase mobility classification. We first present results on unconjugated Au-NPs and then proceed to functionalized Au-NPs. From the change in particle mobility upon SAM Au-NP functionalization, we estimate the surface packing density of SAM molecules on the Au surface. Finally, we estimate the binding energy of alkanethiol molecules on Au-NPs by thermally desorbing alkanethiol molecules from Au-NPs and measuring the corresponding changes in particle mobility. A unique advantage of our approach is that the thermal desorption studies can be conducted on size-selected NPs.

3.1. Unconjugated Au Nanoparticles. *3.1.1. Particle Size Distribution and the Effect of Salt Residues.* Figure 2a presents size distributions obtained by electrospraying as-received citrate-stabilized Au-NP samples of nominal diameters of 10, 30, and 60 nm without any additional sample preparation. For nominally 10 nm sized Au particles, an individual peak is observed at $\sim$14 nm. However, for both of the 30 and 60 nm samples, two peaks are observed: One close to the expected nominal particle size (29 or 58 nm, respectively) and another peak of much higher intensity centered at $\sim$11–12 nm. Deposition of the electrosprayed particles onto a TEM grid confirmed, as shown in Figure 2b, that they are two distinctly different sizes with different image contrasts. The larger particles (dark ones) in the TEM images corresponded to the nominal peak size of the Au-NPs, and the smaller particles (light ones) corresponded to the "extra" much smaller peak seen in the 30 and 60 nm cases. Furthermore, the smaller particles in the TEM are clearly much more numerous, consistent with the DMA/CPC results.

We attribute the peak observed at ca. 11–12 nm to salt remnants in the Au colloid solution. Commercially available aqueous colloidal gold suspensions, like the ones used in the present study, are often stabilized using sodium citrate. XPS characterization of dried films of unconjugated Au colloids confirmed the presence of Na (1071.9 eV) and the presence of a C 1s peak at 289.1 eV, shifted 3.9 eV from the main elemental hydrocarbon peak at 285.2 eV, a binding energy characteristic of carbon in carboxylic acid moieties as would be expected for sodium citrate[25] (Figure S1a, Supporting Information). In addition, transmission FTIR spectra of unconjugated Au colloid dried films revealed
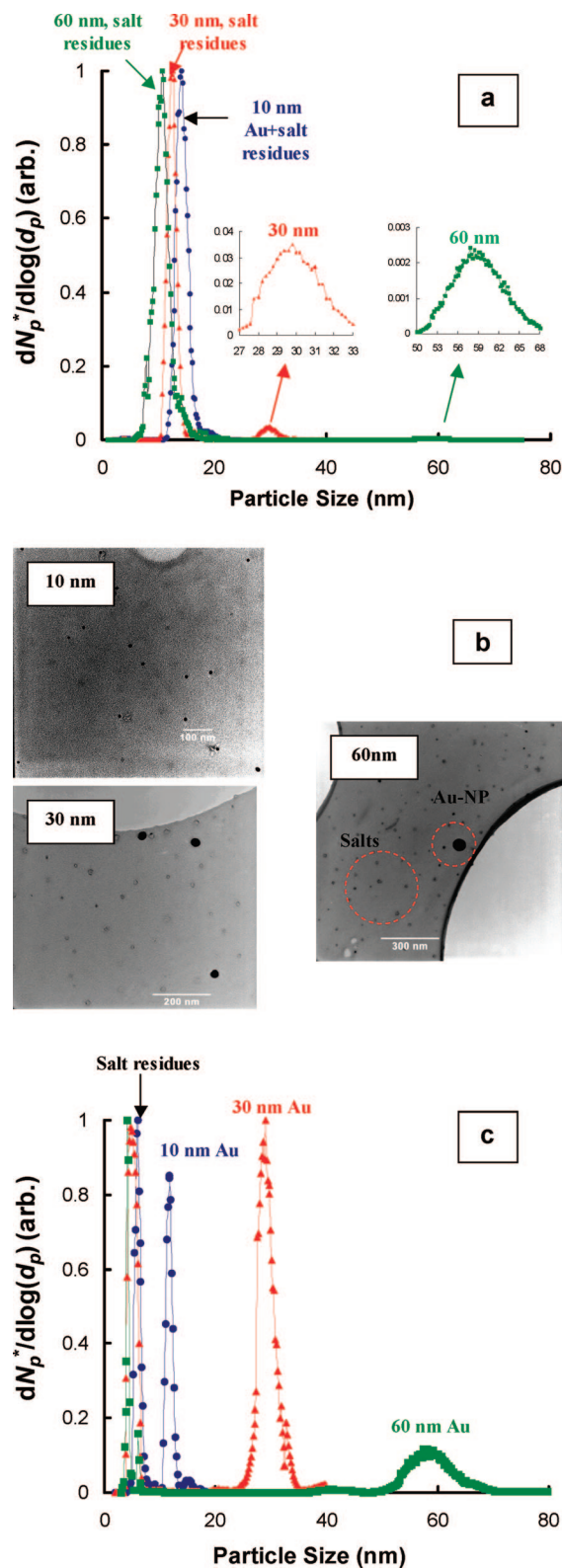

Figure 2. (a) Particle size distribution with 10 nm particles (●), 30 nm (▲), and 60 nm (■). All three sized Au nanoparticles are as-received samples (unconjugated and uncleaned). N_p is the number concentration of particles based on their electrical mobility, and $N_p{}^* = N_p/N_{p,salt\ residues}$. $dN_p{}^*/d\ log(d_p)$ vs d_p represents the log-normal size distribution.[30] (b) TEM images of samples shown in (a). (c) Particle size distribution of samples shown in (a) after centrifuge cleaning.

symmetric and asymmetric carboxylate ion stretches observed at 1381 and 1560 cm^{-1}, respectively, that are attributed to citrate ions used to stabilize the colloidal gold (Figure S2, Supporting

(22) Liao, Y. C.; Roberts, J. T. *J. Am. Chem. Soc.* **2006**, *128*(28), 9061–9065, Self-assembly of organic monolayers on aerosolized silicon nanoparticles.

(23) Higgins, K. J.; Jung, H. J.; Kittelson, D. B.; Roberts, J. T.; Zachariah, M. R. *J. Phys. Chem. A* **2002**, *106*(1), 96–103, Size-selected nanoparticle chemistry: Kinetics of soot oxidation.

(24) Kaufman, S. L. *Anal. Chim. Acta* **2000**, *406*(1), 3–10, Electrospray diagnostics performed by using sucrose and proteins in the gas-phase electrophoretic mobility molecular analyzer (GEMMA).

(25) Moulder, J. F., *Handbook of X-ray Photoelectron Spectroscopy*. Physical Electronics, Inc.: Eden Prairie, MN, 1995.

Table 1. Summary of Particle Sizes for Unconjugated Au Nanoparticles[a]

nominal size (nm)	as-received NPs			processed NPs		
	$d_{p,m}$ (nm)	d_s (nm)	d_{p0} (nm)	$d_{p,m}$ (nm)	d_s (nm)	d_{p0} (nm)
10	14.2	14.2	N/A	10.8	5.0	10.4
30	29.8	12.6	29.0	29.0	4.8	29.0
60	58.4	10.8	58.3	58.2	4.2	58.2

[a] $d_{p,m}$ and d_s are the particle mobility size of Au and salt-residue particles measured in Figure 2b (as-received) and Figure 2c (processed). d_{p0} is the particle size of bare Au after the correction of salt residues on Au surface.

Information). On the basis of these results, we conclude that the peaks seen at <10 nm in Figure 2 originate from the nonvolatile sodium citrate salts in the commercial Au colloid solution.

Thus, in systems containing a nonvolatile soluble salt and Au-NPs, the ES generates two kinds of droplets. One droplet contains Au-NP and salt, which upon solvent evaporation leads to a salt encrusted Au-NP. The other simply contains dissolved salt, so that upon solvent evaporation the remnant becomes a small salt NP. From knowledge of the Au-NP concentration in solution, the droplet diameter, and the generation rate, we can obtain the ratio of the concentration of the two types of drops. From the measured size of the salt remnant particle we can deduce the concentration of the nonvolatile component in the Au-NP containing drop. For example, given the salt NP was measured to be ∼12 nm, the volume fraction of salt on the Au-NP was estimated to be ∼61% for 10 nm, ∼7% for 30 nm and ∼1% for 60 nm samples. Thus, size measurement of smaller Au-NPs is more severely affected by salt formation than that for larger Au-NPs.

To limit salt particle formation and, thus, interference from salt at small NP sizes (i.e., the nominally 10 nm diameter Au-NPs), a "cleaning" procedure was developed. Au-NPs were centrifuged and the supernatant containing excess salt was removed. The Au-NPs were then resuspended with aqueous ammonium acetate solution, a volatile salt, to obtain the necessary conductivity. However, due to the essential role of citrate ions for stabilizing unconjugated Au-NP in solution, fast flocculation can occur during multiple centrifuge cleaning processes. Hence, we only conducted centrifuge cleaning once for each unconjugated Au-NP sample, and through this process we were able to effectively dilute the salts without diluting the colloids. Figure 2c shows the size distribution of Au-NPs after centrifugation and resuspension. Now for all three samples, we clearly see two peaks in the particle size distribution, corresponding to the Au-NPs and salt residues. The now distinct salt peak diameter, d_s, decreased from 11 to 12 nm to 4–5 nm after processing. Thus, the volume of the salt particles was reduced by ∼18 times, in reasonable accord with the extent of dilution. A discontinuity often observed at the upper end of the size distribution was due to the ranging of condensation particle counter as the concentration dropped and did not affect the evaluation of particle size.

3.1.2. Estimation of Mobility Size of Bare Au Nanoparticles. We obtained a corrected value for the mobility size of bare Au-NPs, d_{p0}, using eq 2, where $d_{p,m}$ and d_s are mobility sizes measured by DMA of the Au-NP encrusted with salts and the salt NP, respectively.

$$d_{p0} = \sqrt[3]{d_{p,m}^3 - d_s^3} \qquad (2)$$

This expression takes into account the contribution from the salt residue[24] to the Au-NP size and assumes that (1) during the evaporation of an electrosprayed droplet containing a Au-NP, all of the salt residues in a droplet form a coating layer on Au-NP; (2) the salt residues form a salt nanoparticle (salt NP) after solvent evaporation if the droplet does not contain NPs; and (3) the

volume of a Au-NP is negligible compared to the volume of an electrosprayed droplet. Table 1 summarizes the results of this formula for spectra in Figure 2. The table highlights the value of eq 2 to determine the salt-free value of d_{p0}. Indeed, correcting for the volume of the salt crust brings both values of d_{p0} into agreement within the limit of the DMA's resolving power. Hence, eq 2 provides a simple way to obtain the size of bare Au-NPs under different salt concentrations (i.e., with varying d_s). Correcting for small changes in the net particle diameter with salt concentration is absolutely critical to distinguishing the increase in size after SAM functionalization, to be discussed next.

3.2. Conjugated Au Nanoparticles. *3.2.1. Formation of SAM.* Before measuring the thickness of SAM with ES/DMA, we confirmed the presence of the SAMs on the Au-NPs in the colloid phase using FTIR, XPS, and TEM. We reacted two different thiols, MUA (99+%, negatively charged) and TEG (99+%, neutral) with 30 nm Au colloids. The Supporting Information presents the full details of XPS (Figure S1) and FTIR (Figure S2) analysis for these functionalized nanoparticles, the highlights of which we summarize here. Briefly, FTIR characterization of dried films of SAM modified Au-NPs revealed vibrational features consistent with those observed for full monolayer coverage SAMs formed of the same molecules on macroscopic, planar gold surfaces. XPS analysis of dried SAM-modified Au-NP films on indium substrates also confirmed the presence of alkanethiol chemical elements in their expected chemical states after SAM modification. The ratio of S/Au peak intensities measured for modified Au-NPs was comparable with that measured for SAM films formed on macroscopic planar surfaces, suggesting that similar molecular coverages are achieved on both substrates. TEM images (Figure 3a), reveal well-defined spacing between Au nanoparticles, suggesting that both MUA and TEG monolayers create a uniform coating on the Au-NPs to separate the Au-NPs.[26] Combined, the FTIR, XPS, and TEM characterization data suggest the Au-NPs to be fully conjugated by the alkanethiol SAMs.

We hypothesized that the increase in size of the NP after modification with the alkanethiol SAM should be observable with the ES/DMA. Indeed, the size distribution does shift to larger sizes for both MUA- (∼2 nm) and TEG-coated (∼1.7 nm) Au-NPs, as seen in Figure 3b. Thus, we are able to detect the presence of SAM conjugation on the Au-NPs based on the difference in electrical mobility between conjugated and bare Au-NPs in support of the FTIR, TEM, and XPS results. We now use this change in size to obtain the surface packing density of alkanethiol molecules.

3.2.2. Evaluation of Surface Packing Density of SAM. The ability to size coated particles with 0.2 nm precision allows us to derive a reliable correlation between the change in particle size and the surface packing density of alkanethiol molecules within the SAM coating. We define a change in particle size, ΔL,

(26) Giersig, M.; Mulvaney, P. *J. Phys. Chem.* **1993**, *97*(24), 6334–6336, Formation of Ordered 2-Dimensional Gold Colloid Lattices by Electrophoretic Deposition.
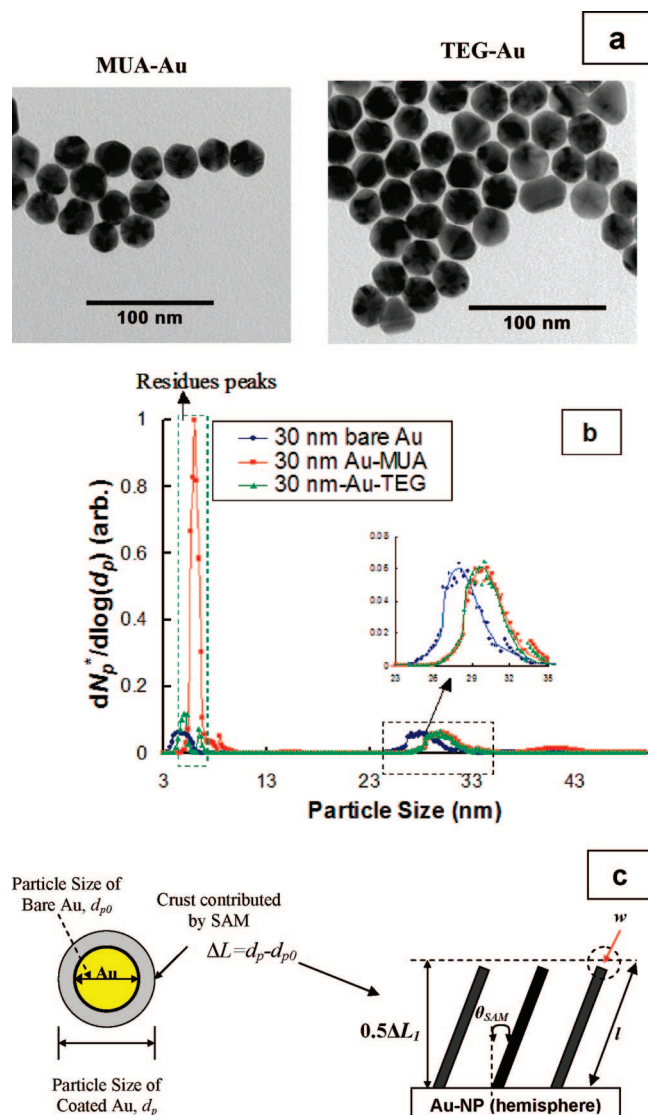
Figure 3. (a) TEM images of conjugated Au-NPs. Particle size was nominally 30 nm. Au-NP were conjugated with MUA (left) and TEG (right). (b) Particle size distribution of Au-NPs with different kinds of SAM-coatings conditions. Blue circles, bare Au-NPs; red squares, MUA-coated Au particles; green triangles, TEG-coated Au particles. For MUA- and TEG-conjugated Au-NPs, peaks appearing at 5–8 nm represent residue particles consisting of salts and unreacted SAM molecules. (c) Conceptual model of SAM-coated Au-NP. l and w are the length and diameter of a cylinder-like SAM molecule, respectively. θ_{SAM} is the tilt angle of SAM molecule normal to the surface.

as $\Delta L = d_p - d_{p0}$ where d_p and d_{p0} represent the coated and uncoated particle mobility diameter, respectively (Figure 3c).

We now consider a simple core–shell model for the change in particle size (ΔL_1), considering only the molecular dimensions of the close-packed SAM normal to the particle surface and neglecting any curvature effects. The length of an alkanethiol molecule, l, is

$$l = a + bN \tag{3}$$

where a is the contribution to the length from the thiol linkage at the Au surface to the SAM terminal functional group, b is the length of repeating methylene (CH_2) group in the SAM backbone, and N is the number of CH_2 groups. Using previously published parameters for MUA,[26–28] $a = 0.3$ nm, $b = 0.127$ nm, and $N =$

(27) Schreiber, F. *Prog. Surf. Sci.* **2000**, *65*(5–8), 151–256, Structure and growth of self-assembling monolayers.

10, the expected length of a MUA molecule is 1.57 nm. ΔL_1 is further refined by recognizing that molecules within a full covered SAM on a 2-D surface typically exhibit an average tilt angle to the surface normal, θ_{SAM}, of 30°.[27] The addition to the diameter of the nanoparticle due to the SAM then becomes

$$\Delta L_1 = 2l \cos(\theta_{SAM}) \tag{4}$$

For MUA, ΔL_1, = 2.72 nm. *Note that this model implies ΔL_1 to be independent of the Au-NP size.*

Comparing theory to experiment, we find ΔL from experiment ($\sim$2.0 nm, Figure 3b) to be 35% lower than the predicted value (ΔL_1, = 2.72 nm), indicating that a SAM-coated Au-NP has a lower drag than other rigid (metal or metal oxides, etc.) core–shell particles. One possible explanation for this discrepancy may be that the SAM coating is not really a dense material. On average the SAM chains have an interchain spacing of $\sim$0.5 nm, about 3–5 times longer than the length of a chemical bond. As such, the surface can be thought of as somewhat porous and the process of energy transfer from gas collisions to the work of drag may differ from that of dense core–shell particles. There is some evidence for this. For example, Shutler et al. via molecular beam experiments observed that a SAM affected gas-surface energy transfer and found that the interaction between SAM chains played a role in the magnitude of the energy transfer. In particular, SAM chains with smaller chain-chain interactions (large-spacing) had greater translational-to-vibrational (TV) energy transfer.[29] At present there is no obvious way to connect the results of changes in TV energy transfer to changes in drag force and therefore the mobility of SAM-coated NPs.

To simplify this problem, we introduce an adjustable parameter, α, to incorporate the effect of SAM spacing in the calculation, and obtain a modified mobility diameter, ΔL_2 ($=\alpha\Delta L_1$).

$$\alpha \equiv \frac{A_2}{A_1} = \frac{N_m wl}{\frac{\pi}{4}[(d_{p0} + \Delta L_1)^2 - d_{p0}^2]} = \frac{4d_{p0}\rho^{0.5}lw}{(2d_{p0} + \Delta L_1)\Delta L_1} \tag{5}$$

where A_1 is the projected area of a rigid, solid shell having a maximal surface packing density of the SAM, A_2 is the effective projected area of the SAM, calculated by assuming molecules occupy a cylinder of length, l, and diameter, w, along the circumference ($A_2 = N_m wl$, where N_m is the total number of SAM molecules along the circumference of Au-NP). N_m is related to the surface packing density of the SAM, ρ, by $N_m = \rho^{1/2}\pi d_{p0}$. For SAM layers on a flat gold surface, $\rho \approx 4.6 \times 10^{14}$ cm^{-2},[27] and for a MUA-coated Au-NP, w was obtained by calculating the width of the COOH group in a MUA molecule ($w = 2 \times (l_{C=O})\sin(\theta_{C=O}) + l_{O-H}$), where $l_{C=O}$ is $\sim$1.43 nm, $\Theta_{C=O}$ is $\sim$50°,[28] and l_{O-H} is $\sim$0.1 nm. Hence, w becomes $\sim$0.23 nm. In summary, increasing α increases the surface packing density, ρ, and thus ΔL_2 is increased. Taking the limit of eq 5 at constant packing density finds $\alpha \rightarrow 0$ as $d_{p0} \rightarrow 0$, whereas $\alpha \rightarrow 1.15\rho^{0.5}w$ was $d_{p0} \rightarrow \infty$. Hence, a size-dependent behavior on ΔL_2 may be observed over a certain range of particle sizes.

In the following, we compare ΔL_2 to our experimental data for MUA-coated particles. We chose four different sized nanoparticles, 10, 20, 30, and 60 nm with a MUA-coating for the comparison. Figure 4 shows the ES-DMA mobility size

(28) Nuzzo, R. G.; Dubois, L. H.; Allara, D. L. *J. Am. Chem. Soc.* **1990**, *112*(2), 558–569, Fundamental-Studies of Microscopic Wetting on Organic-Surfaces 0.1. Formation and Structural Characterization of a Self-Consistent Series of Polyfunctional Organic Monolayers.

(29) Shuler, S. F.; Davis, G. M.; Morris, J. R. *J. Chem. Phys.* **2002**, *116*(21), 9147–9150, Energy transfer in rare gas collisions with hydroxyl- and methyl-terminated self-assembled monolayers.

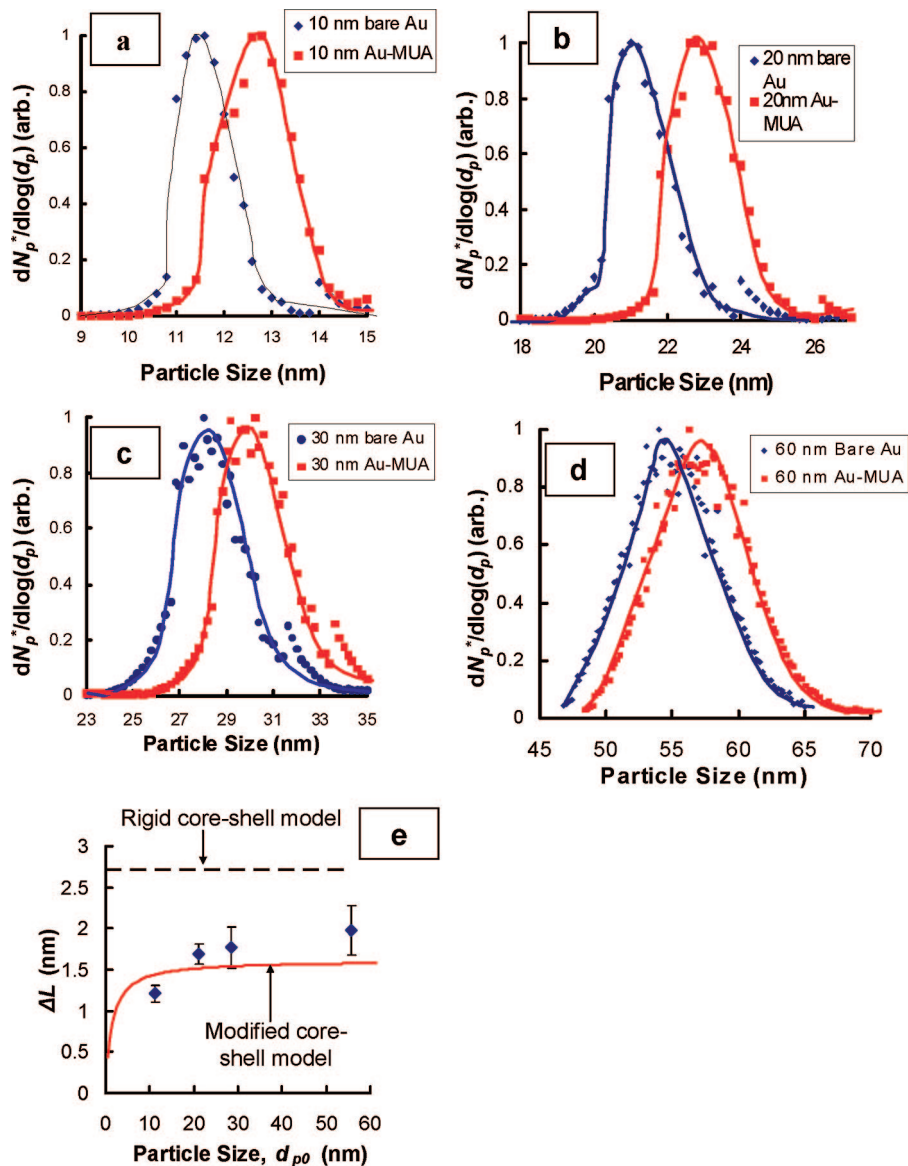(30) Hind, W. C. *Aerosol Technology*, 2nd ed.; Wiley: New York, 1998.

Figure 4. Particle size distributions of bare vs MUA-coated Au-NP for (a) 10 nm particles (b) 20 nm (c) 30 nm, and (d) 60 nm. (e) Comparison of predicted ΔL from experiment (diamonds) with theory (ΔL_1 as dashed line and ΔL_2 as solid line).

distributions for each NP size before and after coating. For each size we clearly observe an increase in peak size after coating with MUA. After correcting for the residual salt crusts, we can determine the increase in the number-averaged particle size[30] to be ~1.2 ± 0.1 nm for 10 nm particles (Figure 4a), 1.7 ± 0.1 nm for 20 nm particles (Figure 4b), ~1.8 ± 0.3 nm for 30 nm particles (Figure 4c), and ~2.0 ± 0.3 nm for 60 nm particles (Figure 4d). These data are plotted in Figure 4e, which show that changes in ΔL to be particle size dependent. This figure also compares ΔL_2 predicted by our modified core–shell model (solid) to the experimental measurements (diamonds). The modified core–shell model reasonably describes the observed changes in mobility size with MUA modification as a function of NP size. While the model is clearly simplistic, it does provide a framework from for studying changes to SAM layers as will be discussed in the next section. Our results also suggest the nature of momentum and energy transfer to "soft" coated NPs is not fully understood and deserves further study.

3.2.3. Temperature-Programmed Desorption of SAMs. We now employ the change in thickness to measure the thermal desorption of the alkanethiol SAMs from Au-NPs. Prior studies have reported on thermal stability values for SAMs on either macrosopic, planar Au surfaces, or large Au clusters. Terrill et. al[31] conducted thermal gravimetric analysis (TGA) of a SAM-coated Au cluster and observed that SAMs were removed from Au clusters at temperatures between 230 and 310 °C. These results are consistent with the observations by Schreiber[27] and Nishida et al.[32] who used temperature-programmed desorption (TPD) analysis to monitor the extent of desorption on planar Au surfaces. To our knowledge, the thermal stability of SAMs on individual Au-NPs remains largely unexplored.

With the ability to distinguish changes of 0.2 nm, ES-DMA offers the opportunity to measure the change in diameter from the thermal desorption of SAMs to gain insight into thermal stability and binding energy. One major advantage of using a gas-phase approach for thermal desorption studies is that thermal processing can be done rapidly and in the absence of complicating

(31) Terrill, R. H.; Postlethwaite, T. A.; Chen, C. H.; Poon, C. D.; Terzis, A.; Chen, A. D.; Hutchison, J. E.; Clark, M. R.; Wignall, G.; Londono, J. D.; Superfine, R.; Falvo, M.; Johnson, C. S.; Samulski, E. T.; Murray, R. W. *J. Am. Chem. Soc.* **1995**, *117*(50), 12537–12548, Monolayers in three dimensions: NMR, SAXS, thermal, and electron hopping studies of alkanethiol stabilized gold clusters.
(32) Nishida, N.; Hara, M.; Sasabe, H.; Knoll, W. *Jpn. J. Appl. Phys., Part 1* **1996**, *35*(11), 5866–5872, Thermal desorption spectroscopy of alkanethiol self-assembled monolayer on Au(111).
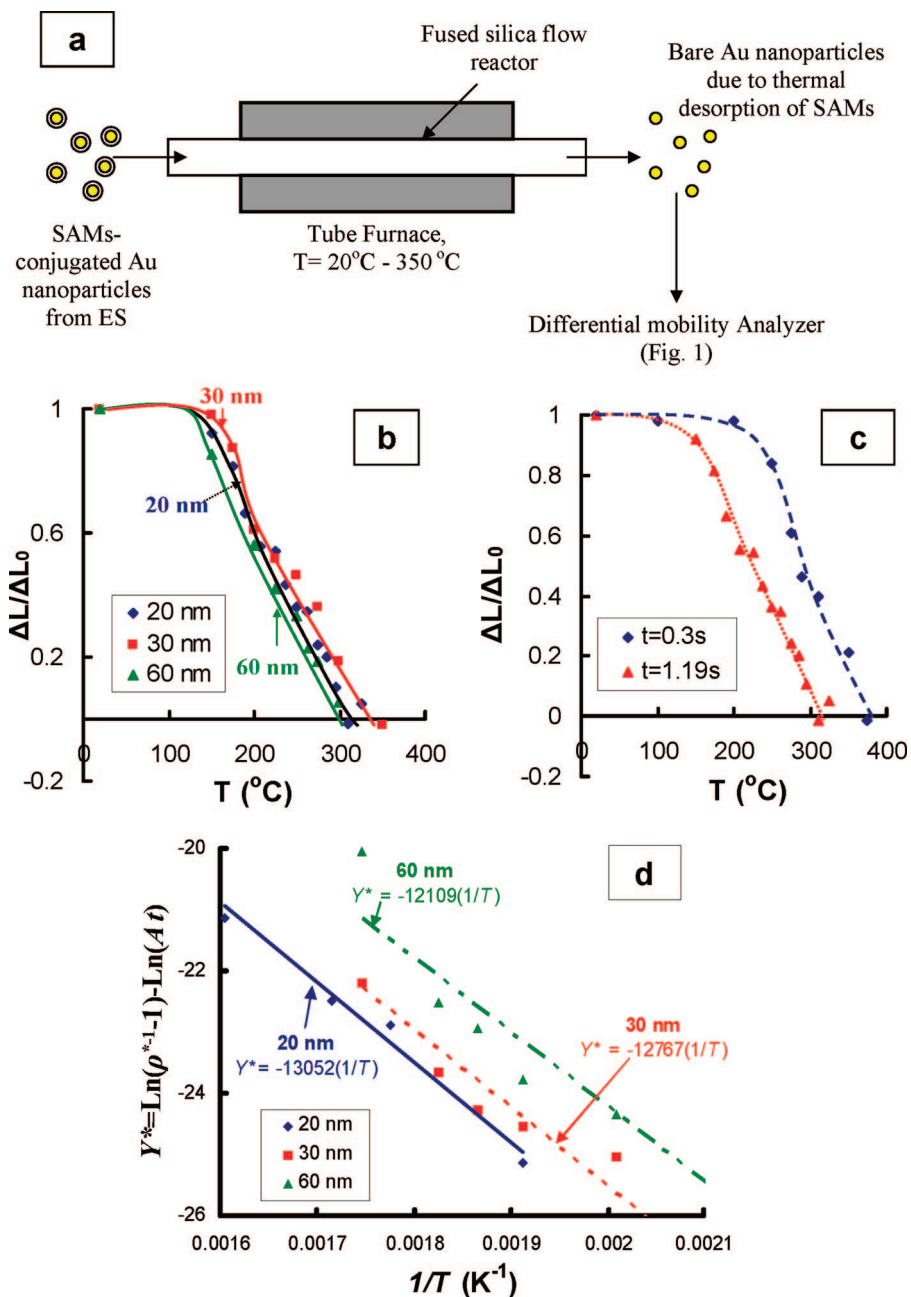
Figure 5. (a) Schematic of the TPD experiment. (b) ΔL^* ($=\Delta L/\Delta L_0$) vs T for MUA-modified Au nanoparticles of three different nominal sizes, 20, 30, and 60 nm. $t = 1.2$ s. (c) ΔL^* vs T for two different residence time, $t = 0.3$ and 1.2 s for 20 nm Au-NPs. (d) Arrhenius plots for three different sizes of Au-MUA particles. $T = 200–350$ °C. $t = 0.3$ s for 20 nm Au-NPs and $t = 1.2$ s for both 30 and 60 nm Au-NPs. $Y^*=\mathrm{Ln}(\rho^{*-1} - 1) - \ln(At)$. The slope $= -E/R$. $R =$ gas constant (8.314 J mol^{-1} K^{-1}).

heat transfer and substrate effects. In particular, the temperature of the particles is well known (i.e., the temperature of the gas) due to their small thermal mass.

In this work, we carried out in situ TPD characterization of MUA-modified Au-NPs using our ES-DMA system, as depicted in Figure 5a. Conjugated nanoparticles generated from the ES process were carried into a flow reactor, heated to various temperatures between 20 and 400 °C for residence times ~0.3–1.2 s, and then sent directly to the DMA for mobility size characterization.

Figure 5b and c shows the change in ΔL as a function of reactor temperature. This figure shows a monotonic decrease in the apparent coating thickness with increasing temperature, where T is the temperature of the Au-NP, t is the reaction time, and ΔL_0 represents ΔL at the initial condition ($T = T_0 = 20$ °C, $t = 0$).

For all particles at the same reaction time (Figure 5b, $t \approx 1.2$ s), we observed that MUA was effectively fully removed from the gold surface at $T = 300–350$ °C independent of particle size. To confirm that this size change is due to SAM desorption and not Au evaporation, we conducted the same heating protocol on bare Au-NPs to confirm that the size change was negligible (for 20 nm bare Au-NPs, $\Delta L \approx 0.2$ nm for $T = 200 – 300$ °C). Considering the effect of reaction time (Figure 5c, 20 nm particles), we observed that the required temperature for full desorption ($\Delta L/\Delta L_0 = 0$) increased from ~300–325 to ~375 °C when the residence time decreased from 1.19 to 0.3 s, indicating that the desorption temperature increased with increasing heating rate. The relatively high temperature of desorption confirms that the MUA is chemisorbed to the surface rather than physisorbed ($T < 80$ °C).[27]

From the observed change of $\Delta L/\Delta L_0$ we can determine the change in the surface packing density of the SAM on an Au-NP. We first define a normalized surface packing density, ρ^* ($\rho^* \equiv \{\rho(T)/\rho_0\}$, where ρ_0 is the surface packing density of SAM initially), and a normalized change in particle size, ΔL^* ($\Delta L^* \equiv \{\Delta L(T)/\Delta L_0\}$), where $\rho(T)$ and $\Delta L(T)$ represent ρ and ΔL under various temperature conditions, respectively. For the size range we considered, our model provides a simple correlation between ΔL, which we measure, and ρ^*, which we use to determine the binding energy in normalized terms,

$$\rho^* = (\Delta L^*)^2 \tag{6}$$

With eq 6, we evaluate the extent of thermal desorption of the SAM simply from the change of ΔL measured by the DMA.

Nishida et al. describe the desorption rate, D_r, of MUA from a flat gold surface as a second-order reaction, and we adopt their description here for the gold particle and check for consistency.[32] The second-order desorption involves a dimerization process of SAM molecules at higher temperature ($T > 200$ °C), when the surface packing density is high.[32,33]

$$D_r = -\frac{d\rho^*}{dt} = k_1(\rho^*)^2 \tag{7}$$

Using eq 7 and the Arrhenius form of k_1, we may evaluate the apparent binding energy (E) of MUA on Au from the TPD results. We set the initial condition as $\rho = \rho(T_0)$ at $t = 0$,

$$\ln\left(\frac{1}{\rho^*} - 1\right) = \ln(At) - \frac{\Delta E}{RT} \tag{8}$$

where k_1 is the rate constant ($=Ae^{(-E/RT)}$), A is the Arrhenius factor, and E is the activation energy. Fitting our TPD data for the temperature range between 200 and 350 °C to eq 8 in Figure 5d shows that a second-order Arrhenius model fits the data well and yields an Arrhenius factor of 1.0×10^{11} s^{-1} with an activation energy $E \approx 105 \pm 10$ kJ/mol for all three sizes of Au-NPs. Thus, for the range of sizes we considered, the curvature effect on

desorption kinetics would seem to be negligible as each MUA molecule only has an arc of 4° or less on the Au surface. Another possible explanation for the absence of a surface curvature effect is that the Au-NPs of this size range may be faceted. This result implies binding of SAMs to Au-NP, at least for $d_{p0} \geq 10$ nm, to be curvature independent.

Accordingly, the energetics we observed are essentially consistent with the work on flat surfaces, where for example, Schreiber[21] observed the activation energy for the desorption from a flat Au surface to be ~126 kJ/mol, which is close to the value, ~115–140 kJ/mol, observed by Nishida et. al.[32,33] Both these measurements are only slightly higher than our 105 kJ/mol result, indicating that binding on the NP may not be significantly different from that observed on a flat surface.

4. Conclusion

We have demonstrated a systematic approach to characterize SAMs of alkanethiol molecules on Au-NPs with ES-DMA. The mobility measurement using a DMA has sufficient resolution to track both the packing density of SAMs and thermally induced desorption kinetics of SAMs from Au-NPs. For the size range (10–60 nm) of MUA-conjugated Au-NPs we considered, the curvature effect on SAM binding is evidently negligible and the binding energy is consistent with similar studies of SAMs on flat surfaces. This study suggests the ES-DMA to be a useful tool for the study of packing density and stability of coatings on nanoparticles.

Disclaimer

Commercial equipment, instruments, or materials identified in this report does not imply recommendation or endorsement by the University of Maryland or the National Institute of Standards and Technology.

Supporting Information Available: XPS and FTIR analysis of nanoparticles. This material is available free of charge via the Internet at http://pubs.acs.org.

LA7024846

(33) Nishida, N.; Hara, M.; Sasabe, H.; Knoll, W. *Jpn. J. Appl. Phys., Part 2* **1996**, *35*(6B), L799–L802Dimerization process in alkanethiol self-assembled monolayer on Au(111).